Emergence of molecular friction in liquids: bridging between the atomistic and hydrodynamic pictures

Arthur V. Straube,[1,2] Bartosz G. Kowalik,[3] Roland R. Netz,[3] and Felix Höfling[1,2]
[1)] *Freie Universität Berlin, Department of Mathematics and Computer Science, Arnimallee 6, 14195 Berlin, Germany*
[2)] *Zuse Institute Berlin, Takustr. 7, 14195 Berlin, Germany*
[3)] *Freie Universität Berlin, Department of Physics, Arnimallee 14, 14195 Berlin, Germany*

Friction in liquids arises from conservative forces between molecules and atoms. Although the hydrodynamics at the nanoscale is subject of intense research and despite the enormous interest in the non-Markovian dynamics of single molecules and solutes, the emergence of friction from the atomistic scale so far could not be demonstrated. Here, we fill this gap based on frequency-resolved friction data from high-precision simulations of three prototypical liquids, including water. Combining with rigorous theoretical arguments, we show that friction in liquids is non-local in time and emerges abruptly at a characteristic frequency, beyond which viscous liquids appear as non-dissipative, elastic solids. At the same time, the molecules experience Brownian forces that display persistent correlations and long-lasting memory. A critical test of the generalised Stokes–Einstein relation, mapping the friction of single molecules to the viscoelastic response of the macroscopic sample, disproves the relation for Newtonian fluids, but substantiates it exemplarily for a supercooled liquid. The employed approach is suitable to yield novel insights into vitrification mechanisms and the intriguing mechanical properties of soft materials.

Molecular friction is a key ingredient for dynamic processes in fluids: it limits diffusion, governs dissipation, and enables the relaxation towards equilibrium. In a liquid environment, the friction experienced by solvated molecules and nanoprobes exhibits a delayed response to external stimuli, indicating non-Markovian dynamics[1–4]. Such memory is found on sub-picosecond up to microsecond scales; it has repercussions on macromolecular transition rates[5–7] and is manifest in the visco-elastic behaviour of soft materials[8–11]. However, the origin of friction from conservative forces between molecules and atoms remains as one of the grand challenges of the physics of fluids[12–15].

Stokes's friction law, describing the resistance to a steadily dragged immersed sphere of radius a, links the friction ζ_0 to the (macroscopic) shear viscosity η_0, and the relation $\zeta_0 = 6\pi\eta_0 a$ scales down remarkably well to single molecules[16,17]. Stokes's hydrodynamic treatment[18] from 1851 was actually more general and addressed slow oscillatory motions in viscous fluids, motivated by inaccuracies of pendulum clocks caused by air flow (fig. 1a). These predictions of a *dynamic* friction $\zeta(\omega)$ that depends on the oscillation frequency ω have been interpreted in terms of a delayed response, also referred to as hydrodynamic memory, and have only recently been shown to be quantitative also for micron-sized particles[1,2]. In the domain of microrheology, measurements of $\zeta(\omega)$ are used to infer the mechanical properties of complex fluids[19–23].

From the perspective of individual molecules or atoms, fluids are governed by conservative interactions and obey Newton's equations of motion, yielding smooth and time-reversible trajectories (fig. 1c). In particular, a single molecule is not subject to friction in this picture, and the mechanism of the required entropy production is far from obvious. Macroscopic friction and other transport coefficients have been linked to microscopic chaos and the Lyapunov spectrum of the liquid[24–26], yet the connection to the corresponding Green–Kubo integrands, or equivalently, to the dynamic friction $\zeta(\omega)$, is an open issue[25]. First-principle theories to friction are hampered by the fact that liquids are strongly interacting systems. For example, a rigorous short-time expansion of the motion at all orders yields zero friction (see Methods). Theoretical progress was made for hard-sphere fluids, where billiard-like collisions generate an instantaneous, Markovian contribution to friction[27], thereby rendering the frictionless regime inaccessible.

To gradually bridge between the atomistic and hydrodynamic regimes, one would ideally like to have a magnifying glass that allows for zooming from the slowest to the fastest processes, thus obtaining an increasingly sharper view of the molecular details (fig. 1a). Spectral quantities such as $\zeta(\omega)$ can serve this purpose with the frequency ω as the control knob. Here, we implemented this idea for three distinct liquids and have traced the friction of molecules over wide frequency windows from fully-developed dissipation all the way down to the non-dissipative regime, revealing sizable variations of $\zeta(\omega)$. Such deviations of $\zeta(\omega)$ from a constant friction ζ_0 signify non-Markovian motion that is widely cast in the generalised Langevin equation [Methods, eq. (1)], parametrised by an associated memory function $\gamma(t)$. The quantities $\zeta(\omega)$ and $\gamma(t)$ are related to each other by a cosine transform, but the determination of either of them from data is a formidable challenge, with substantial progress recently[28–34]. Reaching the high-frequency regime was precluded so far by practical limitations, e.g., statistical noise and insufficient dynamic windows, which we have overcome here by high-precision simulations and an advanced data analysis that utilises physical principles.

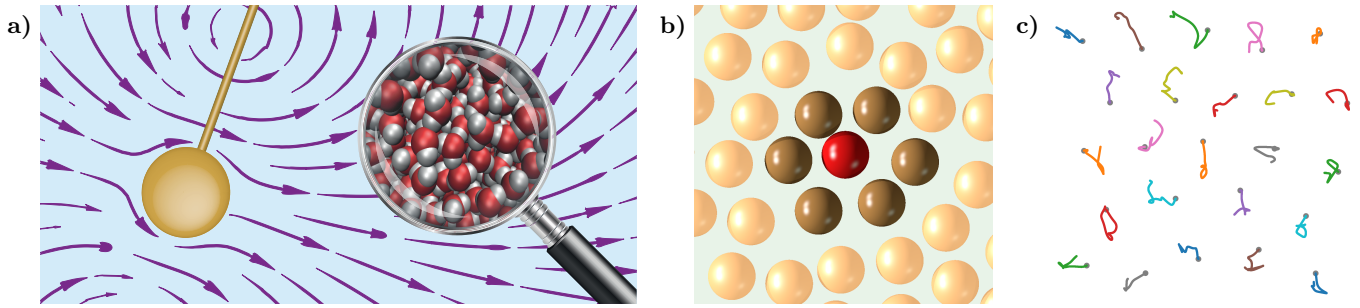

FIG. 1. **Dynamic friction bridges between the hydrodynamic and atomistic pictures of liquids.** Panel (a): A pendulum that oscillates in a viscous fluid with frequency ω experiences a dynamic friction $\zeta(\omega)$ as calculated by Stokes (1851) for slow motion. The associated flow pattern (stream lines) leads to hydrodynamic memory of the motion. Magnifying the microscopic scale, the fluid consists of molecules that obey Newton's equations, which are non-dissipative and generate smooth trajectories. Stokes's result for the pendulum scales down to single molecules, and the function $\zeta(\omega)$ provides the bridge between the frictionless (microscopic) and the hydrodynamic (macroscopic) descriptions. Panels (b,c): In liquids, molecules rattle in transient cages formed by their neighbours (brown spheres); the corresponding short-time trajectories are smooth, but chaotic curves (panel c). The onset of friction is driven by the momentum transfer to the cage, as supported by control simulations of a single particle (red sphere) in a matrix of pinned particles (brown and yellow). Illustration for a mono-atomic fluid in two dimensions.

Instead of observing the response to an oscillatory force, we recorded the Brownian position fluctuations in equilibrium and link them to the friction, taking advantage of a fluctuation dissipation relation. We carried out molecular dynamics simulations for liquid water, for a dense Lennard-Jones (LJ) fluid representing a simple, mono-atomic liquid, and for a supercooled binary mixture serving as a model glass former (see Methods). From the mean-square displacement (MSD) as sole input, we estimated both the dynamic friction $\zeta(\omega)$ and the memory function $\gamma(t)$ in an ansatz-free approach, following two complementary routes that allow for cross-validation (see fig. 2 and Methods). The first route invokes complex analysis and is based on the Fourier–Laplace transform of correlation functions, sampled on a sparse time grid ("adapted Filon algorithm"). Second and independently, we computed the antiderivative of $\gamma(t)$ using a stable deconvolution technique for uniform time grids.

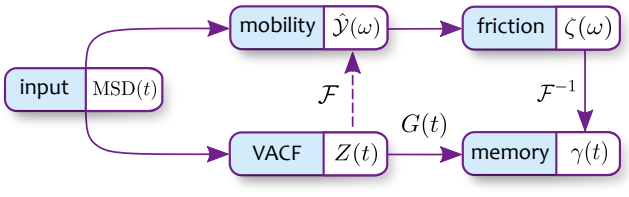

FIG. 2. **Flow chart of the data analysis.** Along the upper route, one starts from the mean-square displacement (MSD) and computes the generalised mobility $\hat{\mathcal{Y}}(\omega)$ by numerical differentiation and a suitable Fourier transform (adapted Filon algorithm); the dynamic friction $\zeta(\omega)$ follows via eq. (7). A Fourier backtransform then yields the memory function $\gamma(t)$. The latter can be obtained more directly along the lower route, which is based on the velocity autocorrelation function (VACF) $Z(t)$ and employs a deconvolution in time domain.

RESULTS

Molecular friction in liquids emerges rapidly. Although all three liquids display rather different dynamics, leaving distinct fingerprints in their friction spectra, their high-frequency behaviours of $\zeta(\omega)$ share significant similarities (fig. 3a–c). Most remarkably, we have found that beyond a liquid-characteristic frequency, $\omega \gtrsim \omega_c$, the friction $\zeta(\omega)$ goes exponentially fast to zero. Such a rapid spectral variation has to be contrasted to the typical algebraic peaks, i.e., the Lorentz–Debye shape, and we argue in the following that our finding is generic for molecular fluids. Upon decreasing frequency, the onset of friction is followed by liquid-specific behaviour over several decades in time until the hydrodynamic value ζ_0 is established: in water, our results for the friction $\zeta(\omega)$ exhibit a local maximum at $\omega/2\pi \approx 5\,\mathrm{THz}$, followed by a slow increase towards the limiting value ζ_0, which is reached near frequencies of 0.1 THz. For the LJ fluid, $\zeta(\omega)$ varies more smoothly with a global maximum at an intermediate frequency, and ζ_0 is approached slowly from above in accord with the hydrodynamic square-root singularity [eq. (18)], essentially calculated by Stokes already[18]. On theoretical grounds, this feature of $\zeta(\omega)$ is generic for all liquids, yet it is suppressed in our data for the other two liquids due to a small prefactor. In the supercooled liquid, we observe a scale separation by 3 dynamic decades of *(i)* the rapid onset of friction and *(ii)* the slow emergence of the hydrodynamic limit. The second process is associated with cage relaxation, strongly delayed in the glassy state, which suggests that the driving mechanism behind the *onset* of friction is not in the structural relaxation of the fluid. Close to the glass transition, the small-frequency friction ζ_0 is governed by self-similar relaxation processes and obeys asymptotic scaling laws[35,36]; the magnitude (prefactor) of these laws, however, is set at high frequencies.

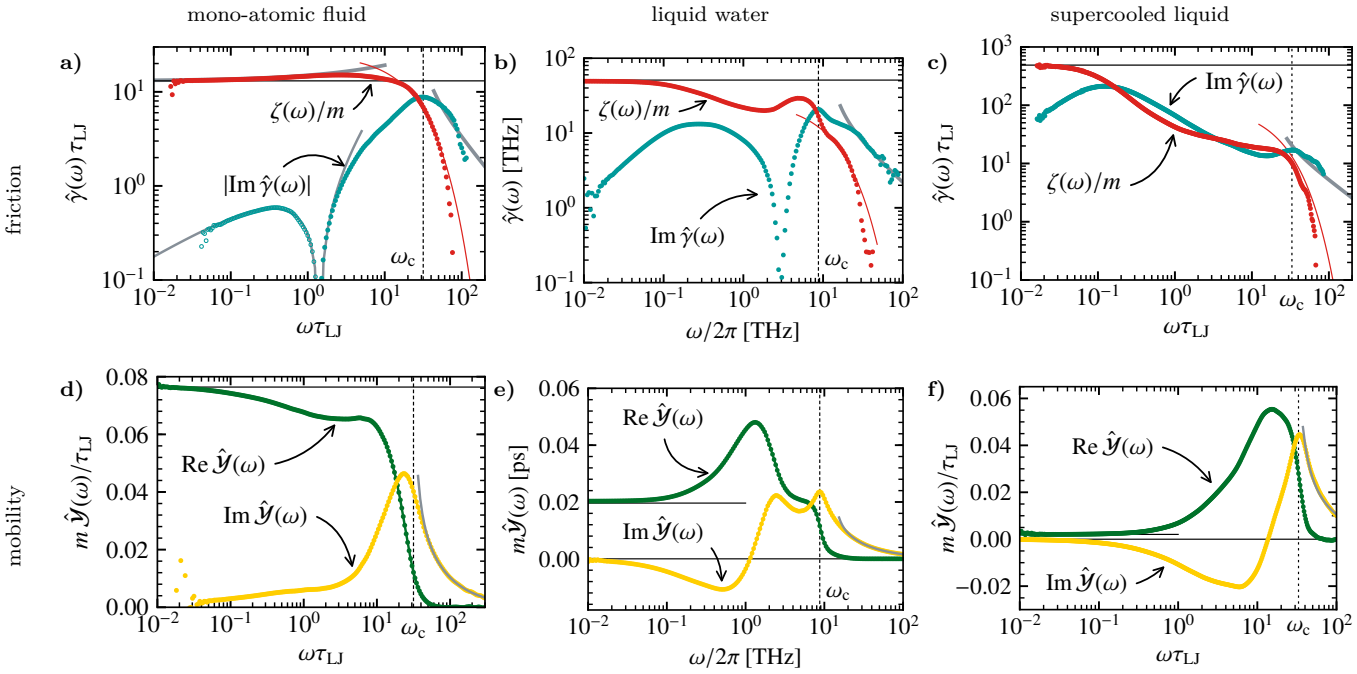

FIG. 3. **Dynamic friction and generalised mobility of three prototypical liquids**. Columns show simulations results for a mono-atomic (LJ) fluid, liquid water, and a supercooled liquid, obtained from the data analysis depicted in fig. 2, with the MSD (not shown) as initial input. Panels (a)–(c): The dynamic friction (red) is the real part of the memory kernel $\hat{\gamma}(\omega)$, as computed from eq. (6). It interpolates between the hydrodynamic value ζ_0/m (horizontal line) and a rapid decrease to zero at high frequencies ($\omega \gg \omega_c$); thin red lines mark exponential decays, $\sim \mathrm{e}^{-\omega/\omega_c}$, to guide the eye. In case of the LJ fluid (panel a), $\zeta(\omega)$ is consistent with Stokes's small-ω asymptote [grey line, eq. (18)], with parameters taken from a fit to the long-time tail of $Z(t)$ (inset of fig. 4a). The elastic response $\mathrm{Im}\,\hat{\gamma}(\omega)$ (turquoise) exhibits a local maximum at high frequencies, defining the characteristic frequency ω_c (vertical lines), and follows the high-frequency asymptote [eq. (15), grey line], with all parameters fixed by short-time fits to the MSD data. The frequency ω_c is close to, but different from the Einstein frequency ω_0. Panels (d)–(f): Numerical results for the generalised mobility $\hat{\mathcal{Y}}(\omega)$, which describes the response to an applied small, oscillatory force (see Methods). The real part $\mathrm{Re}\,\hat{\mathcal{Y}}(\omega)$ (green) approaches the hydrodynamic mobility $1/\zeta_0$ (horizontal line) as $\omega \to 0$ and vanishes rapidly at large frequencies. The imaginary part (yellow) encodes the elastic response, which has a resonance near ω_c (vertical line); at larger frequencies, the data match with theoretical predictions [grey lines, eq. (14)].

Friction depends on the coupling of fast and slow processes. The obtained data of $\zeta(\omega)$ cover the full range of the dynamic response, thereby connecting physics at different scales. Key features will be rationalised by tracing their origins to the dynamics of the fluid particles at short and long times (going backwards in fig. 2). The relevant properties are prominently visible in the second derivative of the MSD, the velocity autocorrelation function (VACF), $Z(t) := \partial_t^2 \mathrm{MSD}(t)/6$, after numerical differentiation with respect to the lag time t (fig. 4a–c). The following should be contrasted to Ornstein's model for Brownian motion, employing a single exponential decay of velocity correlations, $Z(t) \approx v_{\mathrm{th}}^2 \exp(-\zeta_0 t/m)$, which implies a constant (Markovian) friction, $\zeta(\omega) \approx \zeta_0$; by v_{th} we denote the thermal velocity, and m is the molecular mass. As a distinct feature of molecular fluids, obeying Newton's equations, the VACF's true short-time decay is parabola-shaped[17], $Z(t \to 0) \simeq v_{\mathrm{th}}^2\big(1 - \omega_0^2 t^2/2\big)$, introducing the Einstein frequency ω_0. For dense liquids, the VACF, after a sign change, generically displays a regime of anti-correlations, which reflect the transient caging by neighbouring molecules (fig. 1b). For water and the supercooled liquid, these anti-correlations relax slowly with an intermediate power-law decay, $Z(t) \sim -t^{-5/2}$ (insets of fig. 4b,c); such a decay was observed earlier in supercooled liquids[37,38] and it is a well-established long-time tail in colloidal suspensions[39–41] and for diffusion in an arrested, disordered environment[42,43].

The famous long-time tail encoding hydrodynamic memory[17,44,45], $Z(t \to \infty) \sim t^{-3/2}$, is clearly developed in our data for the LJ fluid after another sign change (inset of fig. 4a), and in this situation, Stokes's hydrodynamics describes the slow motion of single molecules (fig. 3a). For the other two liquids studied, the tail is not visible in our data due to a small prefactor, which following mode-coupling arguments decreases as either viscosity or diffusivity increases[17].

The dynamic friction is closely linked to the complex-valued, generalised mobility $\hat{\mathcal{Y}}(\omega)$ via $\zeta(\omega) = \mathrm{Re}[\hat{\mathcal{Y}}(\omega)^{-1}]$. This mobility encodes the response to a small, oscillatory force and is accessible in, e.g., scat-

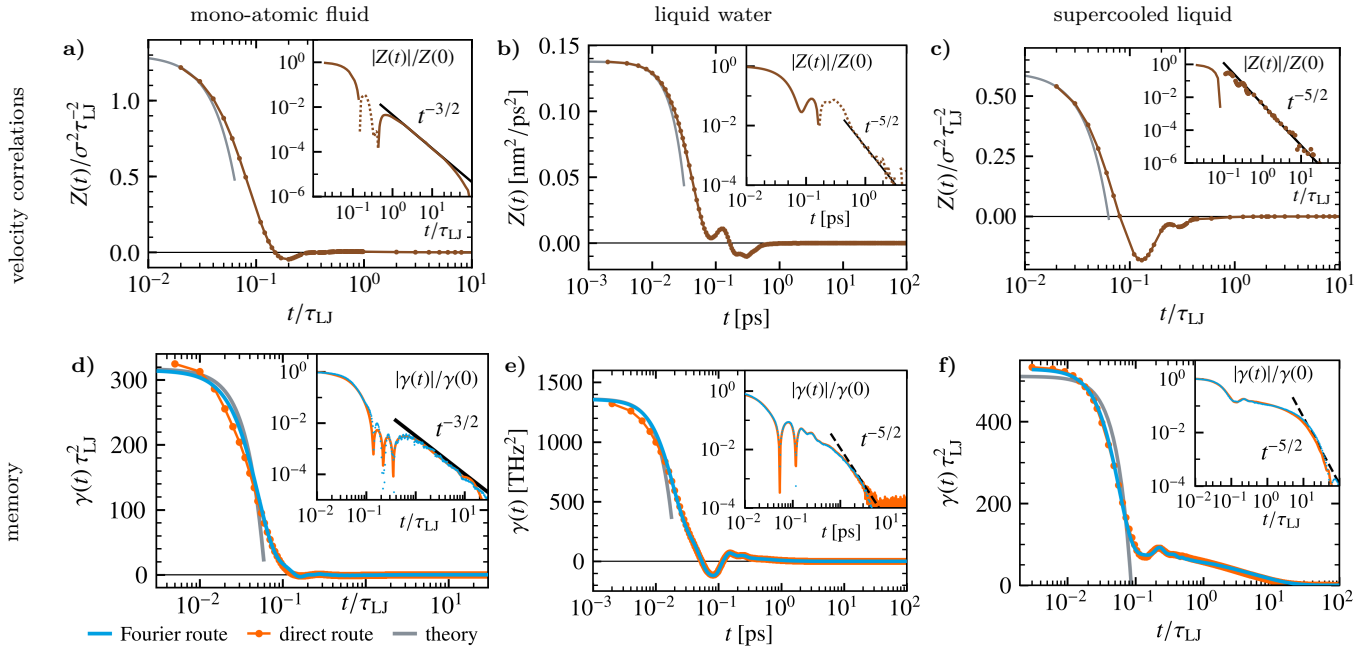

FIG. 4. **Velocity autocorrelators and corresponding memory functions for the three investigated liquids**. Columns show results for a mono-atomic (LJ) fluid, liquid water, and a supercooled liquid. Panels (a)–(c): simulation results for the VACF (brown symbols) display a parabolic decrease at short times (grey lines) and power law decays at long times (insets, negative values are dotted). The VACF is obtained from the second derivative of the MSD with respect to lag time. Panels (d)–(f): The memory function $\gamma(t)$ encodes the autocorrelation of Brownian forces on the molecules [eq. (2)]. For each liquid, $\gamma(t)$ was computed from a cosine transform of $\hat{\zeta}(\omega)$ [blue line, eq. (9)] with input data from fig. 3a–c] and is compared to the deconvolution results in time domain [orange line, eq. (22)]. The data follow the predicted short-time decay eq. (16) (grey line) and exhibit power-law decays consistent with eq. (19) (insets), preceded by an ultra-slow decay in case of the supercooled liquid [panel (f)].

tering experiments[46]. Here, we computed $\hat{\mathcal{Y}}(\omega)$ from the VACF upon employing a fluctuation dissipation relation (see Methods and fig. 3d–f). Our data reveal a generic, rapid decrease of the dissipative part, $\hat{\mathcal{Y}}'(\omega) := \mathrm{Re}\,\hat{\mathcal{Y}}(\omega)$, upon increasing frequency towards the microscopic regime, $\omega \gg \omega_c$; concomitantly, the elastic response, $\hat{\mathcal{Y}}''(\omega) := \mathrm{Im}\,\hat{\mathcal{Y}}(\omega)$, has a resonance near ω_c due to vibrational motion of molecules in their cages. In the low-frequency limit, the reciprocal of the macroscopic friction is recovered, $\hat{\mathcal{Y}}(\omega \to 0) = 1/\zeta_0$. In the examples studied, both regimes are separated by at least two decades in time, which show material-specific features: the mobility of water molecules is 2.5-fold enhanced over its macroscopic value near $\omega/2\pi \approx 1.3\,\mathrm{THz}$; similarly, a factor of 30 is observed for the supercooled liquid. At variance, the hydrodynamic long-time tail, as for the LJ liquid, demands $\hat{\mathcal{Y}}'(\omega \to 0)$ to be approached from below. The interplay of slow and fast processes enters the response $\hat{\mathcal{Y}}(\omega)$, and thus the dynamic friction $\zeta(\omega)$, at all frequencies, which is borne out by the Kramers–Kronig relations. In particular, singular behaviour of $\hat{\mathcal{Y}}''(\omega)$ as $\omega \to 0$ influences the detailed onset of friction at large frequencies.

Friction is non-local in time. The rapid decrease of $\hat{\mathcal{Y}}'(\omega)$ is mathematically justified from the short-time properties of the VACF. Physical molecular trajectories, being solutions to Newton's equations, are smooth and yield a smooth function $Z(t)$; in particular, all derivatives $Z^{(n)}(t)$ exist at $t = 0$ and are finite. Thus, invoking exact sum rules [eq. (10)], all moments of the spectrum $\hat{\mathcal{Y}}'(\omega)$ are finite, which requires an exponentially fast decay as $\omega \to \infty$. Combining with the large-ω asymptote of the imaginary part, $\hat{\mathcal{Y}}''(\omega) \simeq 1/m\omega \gg \hat{\mathcal{Y}}'(\omega)$ (see Methods) and using $\zeta(\omega) = \hat{\mathcal{Y}}'(\omega)/\left[\hat{\mathcal{Y}}'(\omega)^2 + \hat{\mathcal{Y}}''(\omega)^2\right]$ proves that $\zeta(\omega) \simeq (m\omega)^2\,\hat{\mathcal{Y}}'(\omega)$ as $\omega \to \infty$ and thus an exponentially fast suppression of the friction.

It is tempting to use a systematic short-time expansion of $Z(t)$ to predict the large-frequency behaviour of the friction. However, $Z(t)$ being an even function due to time-reversal symmetry in equilibrium renders the large-ω asymptotes zero, $\hat{\mathcal{Y}}'(\omega) \equiv 0$ and thus $\zeta(\omega) \equiv 0$, even if the complete Taylor series of $Z(t)$ in $t = 0$ was known (see Methods). Note that $\hat{\mathcal{Y}}''(\omega)$ and the elastic counterpart of $\zeta(\omega)$ are well captured by such an expansion (fig. 3d–i). This observation underlines that, on all scales, friction emerges as a phenomenon that is non-local in time, i.e., it cannot be anticipated from the local behaviour of the molecular trajectories.

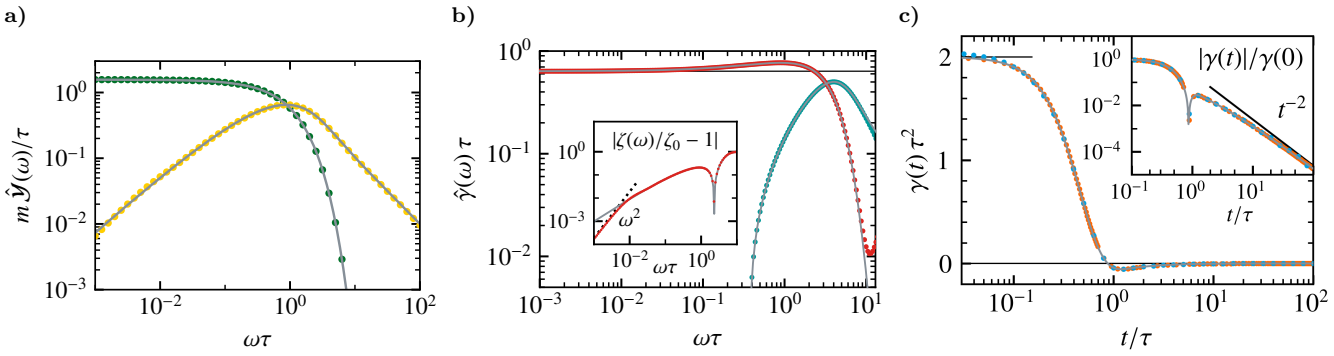

FIG. 5. **Theoretical model justifies exponentially fast onset of friction and persistent memory.** Exact results (grey solid lines) for the VACF model of eq. (20), combining the smoothness and time-reversal symmetry of molecular autocorrelation functions with a long-time tail. As a sensitive test of our numerical procedures, symbols show numerical results from the MSD as input, sparsely sampled on a geometrically spaced grid. The panels show (a) the complex-valued, generalised mobility $\hat{\mathcal{Y}}(\omega)$, (b) the dynamic friction $\zeta(\omega)$ and its elastic counterpart $\mathrm{Im}\,\hat{\gamma}(\omega)$, and (c) the memory function $\gamma(t)$ in time domain. The latter inherits the long-time tail $\sim t^{-2}$ from the VACF, but of opposite sign (inset). The tail induces non-analytic behaviour of $\zeta(\omega)$ at small frequencies, which crosses over to $\sim \omega^2$ due to the smooth, exponential cutoff of the Fourier integrals (inset of panel b). Same colour code as in figs. 3 and 4.

Our numerical and theoretical findings are supported by an analytically solvable example. The choice $Z(t) = v_{\mathrm{th}}^2\left[1 + (t/\tau)^2\right]^{-1}$ combines the smoothness and time reversal symmetry of molecular autocorrelation functions with a long-time tail. It yields an exponential decay of the mobility, $\hat{\mathcal{Y}}'(\omega) \sim \mathrm{e}^{-|\omega\tau|}$ (dissipative part), and hence a rapid suppression of friction, $\zeta(\omega \to \infty) \sim (\omega\tau)^2\mathrm{e}^{-\omega\tau}$, as demanded above (see Methods and fig. 5).

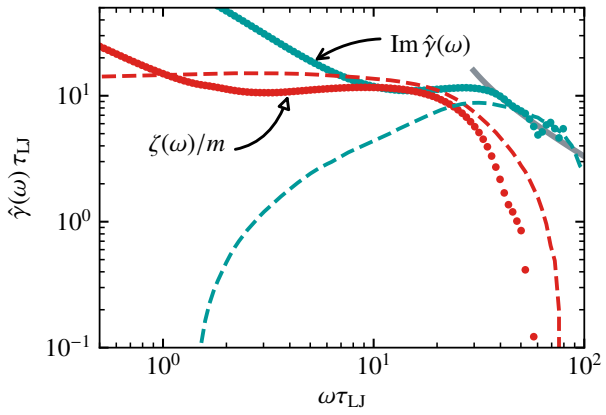

FIG. 6. **Friction emerges due to rattling motion in immobile cages.** Dynamic friction $\zeta(\omega)$ (red symbols) obtained in a control simulation of a single particle moving in a frozen-in cage formed by neighbouring particles (fig. 1b). The setup was created by pinning the particles of the LJ fluid except for one; results correspond to an ensemble average over 10^6 typical cages. The imaginary part of the memory kernel $\hat{\gamma}(\omega)$ (turquoise) ties in with the high-frequency prediction (gray). Dashed lines show the results for the unconstrained fluid at the same conditions for comparison (fig. 3a).

Irreversible momentum transfer drives the onset of friction. A pressing question is about the physical mechanism that generates the onset of friction. Motivated by our results for the supercooled liquid (fig. 3c), we performed a control simulation for the LJ fluid with the structural relaxation switched off by pinning all particles but one. The rattling motion in such a frozen-in cage (fig. 2) experiences a dynamic friction that closely resembles our generic findings for $\zeta(\omega)$ at high frequencies, $\omega \gtrsim \omega_c$ (fig. 6). We conclude that it is the (irreversible) momentum transfer to neighbouring molecules that drives the onset of friction, corroborated by the observation that instantaneous momentum exchange implies a non-zero limit, $\zeta(\omega \to \infty) > 0$, as in the case of hard spheres[27]. The fact that dissipation is linked to trajectories for which the time-reversed path is extremely improbable leads us to speculate that the onset frequency ω_c is intimately related to the largest Lyapunov exponent λ_{max} of the fluid, which is close to, but different from the Einstein frequency ω_0 (ref. 26).

Dynamic friction implies intricate memory of Brownian motion. Within the framework of the generalised Langevin equation [eq. (1)], momentum relaxation is governed by a memory function $\gamma(t)$ that is fully determined by $\zeta(\omega)$ [eqs. (7) and (9)]. At the same time, $\gamma(t)$ is also the autocorrelator of Brownian, random forces on the molecules, up to a constant prefactor, and $\zeta(\omega)$ encodes the corresponding spectrum [eq. (2)]. Within Ornstein's idealised model of Brownian motion, one assumes independent Brownian forces, implying a flat, white spectrum, $\zeta(\omega) \approx \zeta_0$, and a delta-peaked memory function $\gamma(t)$. For molecular liquids, however, the memory functions display a universal parabola-shaped short-time decay [fig. 4d–f and eq. (16)]. For water and the LJ fluid, the short-time regime of $\gamma(t)$ is followed by oscillatory

behaviour including sign changes and, finally, different power-law decays for the two liquids encoding different physics (insets of fig. 4d,e, also see fig. 5c); generally, power-law tails of the memory function are directly inherited from the VACF without a change of exponent [eq. (19)]. For the supercooled liquid, $\gamma(t)$ remains positive and exhibits the onset of a plateau (near $t \approx 0.3\tau_{\mathrm{LJ}}$), which decays logarithmically slowly over 2 decades in time (fig. 4f). From the modelling perspective, it is desirable to approximate the memory functions such that the initial decay, the typical persistence time, and the integral of $\gamma(t)$ are reproduced, the latter yielding ζ_0 [eq. (13)]. For all three liquids, the complexity and the long-lived nature of the memory, however, preclude simple models of $\gamma(t)$ such as the superposition of few exponential decays. The quantitative knowledge of $\zeta(\omega)$, as obtained here, paves the way for more favourable approximations of memory in the frequency domain, which can yield mathematically and physically consistent interpolations of Brownian motion from the fastest to the slowest scales.

Relation to viscosity and elasticity of liquids. Going beyond the dynamics of single molecules and their friction, the relation to the visco-elastic properties of complex fluids is of ongoing interest for the physics of polymers, living cells, and the glass transition. The potentially tight coupling between single-particle and collective responses was phrased as an *ad hoc* extension of Stokes's friction law to the frequency domain, $\zeta(\omega) = 6\pi\,\mathrm{Re}[\hat{\eta}(\omega)]a$, referred to as generalised Stokes–Einstein relation (GSER), which has found wide applications in the context of microrheology experiments[19–22]. It links the dynamic friction $\zeta(\omega)$ of a probe particle to the dynamic shear modulus, $\hat{G}(\omega) = -\mathrm{i}\omega\hat{\eta}(\omega)$, a complex-valued function encoding the stress response of the macroscopic fluid sample to a small, oscillatory shear strain. The generalised viscosity $\hat{\eta}(\omega)$ tends to the hydrodynamic shear viscosity η_0 as $\omega \to 0$, with $\mathrm{Re}\,\hat{\eta}(\omega)$ representing the spectrum of shear stress fluctuations (up to a constant factor) by a fluctuation dissipation relation. Thus, if the GSER holds the single-particle memory $\gamma(t)$ is proportional to the autocorrelator of shear stresses, which means that the Brownian force on the particle and the fluctuation of the shear stress are statistically equivalent variables.

A critical assessment of the validity of the GSER is permitted by comparing our data for $\zeta(\omega)$ to results for $\hat{\eta}(\omega)$, calculated within the same simulations (see fig. 7 and Methods). Generically, the dissipative part, $\mathrm{Re}\,\hat{\eta}(\omega)$, decays exponentially fast as $\omega \to \infty$, which is required by analogous arguments as given for $\zeta(\omega)$ and $\hat{\mathcal{Y}}'(\omega)$. For high frequencies, only the imaginary part survives due to its slow decay, $\hat{\eta}(\omega) \simeq G_\infty/(-\mathrm{i}\omega)$, inducing a non-zero and real-valued modulus, $\hat{G}(\omega \gg \omega_c) \approx G_\infty > 0$. Therefore, our data clearly demonstrate that, indeed, liquids respond to high-frequency shear like a non-dissipative, elastic solid as put forward by the classical work of Frenkel[47]. However, the attempt to predict the elastic modulus G_∞ from the vibrational motion of molecules in their cages, by virtue of the GSER, would considerably overestimate the modulus by factors of ≈ 2 for the liquids studied (fig. 7c,d).

The passage from the elastic to the viscous limit occurs upon decreasing frequency, leading in case of the LJ fluid to a monotonic increase of $\mathrm{Re}\,\hat{\eta}(\omega)$, which, empirically, follows a stretched exponential over almost the full frequency domain (fig. 7a). In particular, $\hat{\eta}(\omega) \approx \eta_0$ is constant for $\omega \lesssim 2\tau_{\mathrm{LJ}}^{-1}$, which defines the hydrodynamic regime. For these frequencies, the single-molecule response is very well described by Stokes's dynamic friction [eq. (18)], making the GSER violation apparent for Newtonian fluids, for which $\hat{\eta}(\omega) = \eta_0$. It is evidenced further by the dissimilarity of the elastic parts, $\mathrm{Im}\,\hat{\gamma}(\omega)$ and $\mathrm{Im}\,\hat{\eta}(\omega)$.

In supercooled liquids, the zero-frequency GSER holds at the scale of molecules, in particular, the ratio ζ_0/η_0 is observed to be constant over a wide temperature range—in line with the mode-coupling theory of the idealised glass transition[36]. At very low temperatures, however, marked deviations from the Stokes–Einstein relation (mostly studied for $\omega \to 0$) have received considerable attention as they signify the opening of additional relaxation channels not included in the standard theory[48–52]. For the supercooled liquid studied here exemplarily, both viscous and elastic responses satisfy the GSER over a wide frequency window (fig. 7b). Notably, the elastic components collapse almost perfectly in this case, $\mathrm{Im}\,\hat{\gamma}(\omega) \sim \mathrm{Im}\,\hat{\eta}(\omega)$, which we attribute to the same (apparent) power law scaling, $\approx \omega^{-0.75}$, at intermediate frequencies. Yet, the collective response lacks the elastic peak of $\mathrm{Im}\,\hat{\gamma}(\omega)$ at ω_c, causing the breakdown of the GSER at large frequencies. This suggests that a future frequency-resolved study of systematic deviations from the GSER upon further supercooling can clarify the separate contributions of fast and slow processes to the decoupling of diffusion and viscosity ("Stokes–Einstein violation") close to the glass transition temperature.

Further perspectives. Molecular friction in liquids arises from a complex interplay of processes on disparate time scales, and the large variability of $\zeta(\omega)$ over orders of magnitude reveals the strongly non-Markovian nature of Brownian motion in liquid environments, with far-reaching implications for nanoscale processes. Examples are as diverse as reaction rates and barrier crossings in macromolecular dynamics[5–7] and flows near liquid–solid interfaces[40,53–55]; the ability to quantify the corresponding memory is vital for their realistic descriptions.

Beyond that, the finding of a generic drop of $\zeta(\omega)$ at a large, liquid-specific frequency ω_c marks the rapid onset of friction, which we attribute to the momentum transfer to neighbouring molecules. These results refine the fundamental question on a quantitative link between friction and microscopic chaos: Whether and how does the frequency-dependence of transport coefficients relate to

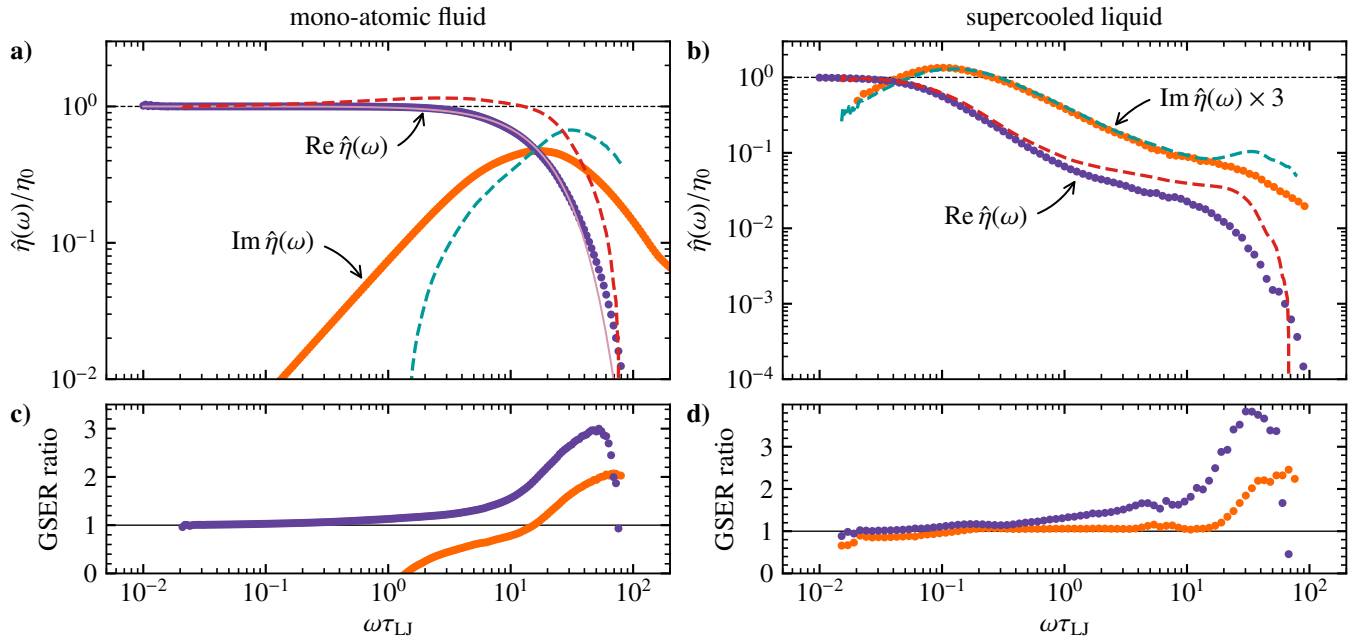

FIG. 7. **Test of the generalised Stokes–Einstein relation (GSER).** Panels (a,b): The generalised viscosity $\mathrm{Re}\,\hat{\eta}(\omega)$ (violet symbols) of the mono-atomic LJ fluid (left column) and the supercooled liquid (right column) is compared to the GSER prediction $\zeta(\omega)/6\pi a$ (red dashed lines), based on the dynamic friction data of single molecules (fig. 3a,c), and correspondingly for the imaginary counterparts of the elastic responses (orange symbols and turquoise dashed lines). The effective particle radius a for each liquid is chosen such that the viscosity and friction curves coincide at $\omega = 0$. The pink solid line in panel (a) is an empirical fit of a stretched exponential, $\mathrm{Re}\,\hat{\eta}(\omega) \simeq \eta_0 \exp(-(\omega/\omega_\eta)^\beta)$ with $\beta = 1.29$ and $\omega_\eta = 1.19\,\omega_0$. In panel (b), the data for the elastic responses are shifted up by a factor of 3 for clarity. Panels (c,d): The GSER is tested by plotting the ratios $\zeta(\omega)/6\pi[\mathrm{Re}\,\hat{\eta}(\omega)]a$ (violet) and $m[\mathrm{Im}\,\hat{\gamma}(\omega)]/6\pi[\mathrm{Im}\,\hat{\eta}(\omega)]a$ (orange); deviations from unity quantify the GSER violation.

the Lyapunov spectrum of the liquid?[24,25]

Methodologically, our ansatz-free approach has immediate applications for the interpretation of high-resolution microrheology data[1–3,22], which requires deducing frequency-dependent moduli from the displacement statistics along the same lines as done here for the dynamic friction. Relying merely on the existence of a steady state [cf. eq. (12)], the developed methodology is not limited to friction, but can be employed also for the analysis of non-Markovian time series from simulation and experiment. It finds novel applications in, e.g., the anomalous diffusion within living cells[11] and the kinetics of chemical reactions[56]. It opens a promising avenue for research on the migration of malignant cells in tissue[57] and on predictive stochastic models of financial market[58] and geographic[59] data.

[1] T. Franosch, M. Grimm, M. Belushkin, F. Mor, G. Foffi, L. Forró, and S. Jeney, "Resonances arising from hydrodynamic memory in Brownian motion," Nature **478**, 8–11 (2011).

[2] S. Kheifets, A. Simha, K. Melin, T. Li, and M. G. Raizen, "Observation of Brownian motion in liquids at short times: Instantaneous velocity and memory loss," Science **343**, 1493–1496 (2014).

[3] J. Berner, B. Müller, J. R. Gomez-Solano, M. Krüger, and C. Bechinger, "Oscillating modes of driven colloids in overdamped systems," Nat. Commun. **9**, 999 (2018).

[4] J. O. Daldrop, B. G. Kowalik, and R. R. Netz, "External potential modifies friction of molecular solutes in water," Phys. Rev. X **7**, 041065 (2017).

[5] T. Guérin, N. Levernier, O. Bénichou, and R. Voituriez, "Mean first-passage times of non-Markovian random walkers in confinement," Nature **534**, 356 (2016).

[6] D. de Sancho, A. Sirur, and R. B. Best, "Molecular origins of internal friction effects on protein-folding rates," Nat. Commun. **5**, 4307 (2014).

[7] J. O. Daldrop, J. Kappler, F. N. Brünig, and R. R. Netz, "Butane dihedral angle dynamics in water is dominated by internal friction," Proc. Natl. Acad. Sci. U. S. A. **115**, 5169–5174 (2018).

[8] P. Sollich, F. Lequeux, P. Hébraud, and M. E. Cates, "Rheology of soft glassy materials," Phys. Rev. Lett. **78**, 2020–2023 (1997).

[9] D. Mizuno, C. Tardin, C. F. Schmidt, and F. C. MacKintosh, "Nonequilibrium mechanics of active cytoskeletal networks," Science **315**, 370–373 (2007).

[10] D. Winter, J. Horbach, P. Virnau, and K. Binder, "Active nonlinear microrheology in a glass-forming Yukawa fluid," Phys. Rev. Lett. **108**, 028303 (2012).

[11] F. Höfling and T. Franosch, "Anomalous transport in the crowded world of biological cells," Rep. Prog. Phys. **76**, 046602 (2013).

[12] E. Secchi, S. Marbach, A. Niguès, D. Stein, A. Siria, and L. Bocquet, "Massive radius-dependent flow slippage in carbon nanotubes," Nature **537**, 210–213 (2016).

[13] F. Perakis, G. Camisasca, T. J. Lane, A. Späh, K. T. Wikfeldt, J. A. Sellberg, F. Lehmkühler, H. Pathak, K. H. Kim, K. Amann-Winkel, S. Schreck, S. Song, T. Sato, M. Sikorski, A. Eilert, T. McQueen, H. Ogasawara, D. Nordlund, W. Roseker, J. Koralek, S. Nelson, P. Hart, R. Alonso-Mori, Y. Feng, D. Zhu, A. Robert, G. Grübel, L. G. M. Pettersson, and A. Nilsson, "Coherent X-rays reveal the influence of cage effects on ultrafast

water dynamics," Nat. Commun. **9**, 1917 (2018).
[14]A. Bylinskii, D. Gangloff, and V. Vuletić, "Tuning friction atom-by-atom in an ion-crystal simulator," Science **348**, 1115–1118 (2015).
[15]P. Gaspard, M. E. Briggs, M. K. Francis, J. V. Sengers, R. W. Gammon, J. R. Dorfman, and R. V. Calabrese, "Experimental evidence for microscopic chaos," Nature **394**, 865–868 (1998).
[16]A. Bartsch, K. Rätzke, A. Meyer, and F. Faupel, "Dynamic arrest in multicomponent glass-forming alloys," Phys. Rev. Lett. **104**, 195901 (2010).
[17]J.-P. Hansen and I. McDonald, *Theory of Simple Liquids*, 3rd ed. (Academic Press, Amsterdam, 2006).
[18]G. G. Stokes, "On the effect of the internal friction of fluids on the motion of a pendulum," Trans. Cambridge Philos. Soc. **9**, 8 (1851).
[19]T. G. Mason and D. A. Weitz, "Optical measurements of frequency-dependent linear viscoelastic moduli of complex fluids," Phys. Rev. Lett. **74**, 1250–1253 (1995).
[20]F. Gittes, B. Schnurr, P. D. Olmsted, F. C. MacKintosh, and C. F. Schmidt, "Microscopic viscoelasticity: Shear moduli of soft materials determined from thermal fluctuations," Phys. Rev. Lett. **79**, 3286–3289 (1997).
[21]T. M. Squires and T. G. Mason, "Fluid mechanics of microrheology," Annu. Rev. Fluid Mech. **42**, 413–438 (2010).
[22]T. A. Waigh, "Advances in the microrheology of complex fluids," Rep. Prog. Phys. **79**, 074601 (2016).
[23]A. Rigato, A. Miyagi, S. Scheuring, and F. Rico, "High-frequency microrheology reveals cytoskeleton dynamics in living cells," Nat. Phys. **13**, 771–775 (2017).
[24]R. Dorfman, *An Introduction to Chaos in Nonequilibrium Statistical Mechanics* (Cambridge University Press, 2003).
[25]E. G. D. Cohen, "Transport coefficients and Lyapunov exponents," Physica A **213**, 293–314 (1995).
[26]H. A. Posch and W. G. Hoover, "Lyapunov instability of dense Lennard-Jones fluids," Phys. Rev. A **38**, 473–482 (1988).
[27]L. Bocquet, J. Piasecki, and J.-P. Hansen, "On the Brownian motion of a massive sphere suspended in a hard-sphere fluid. I. Multiple-time-scale analysis and microscopic expression for the friction coefficient," J. Stat. Phys. **76**, 505–526 (1994).
[28]H. K. Shin, C. Kim, P. Talkner, and E. K. Lee, "Brownian motion from molecular dynamics," Chem. Phys. **375**, 316 – 326 (2010).
[29]F. Gottwald, S. Karsten, S. D. Ivanov, and O. Kühn, "Parametrizing linear generalized Langevin dynamics from explicit molecular dynamics simulations," J. Chem. Phys. **142**, 244110 (2015).
[30]D. Lesnicki, R. Vuilleumier, A. Carof, and B. Rotenberg, "Molecular hydrodynamics from memory kernels," Phys. Rev. Lett. **116**, 147804 (2016).
[31]G. Jung, M. Hanke, and F. Schmid, "Iterative reconstruction of memory kernels," J. Chem. Theory Comput. **13**, 2481–2488 (2017).
[32]H. Meyer, T. Voigtmann, and T. Schilling, "On the non-stationary generalized Langevin equation," J. Chem. Phys. **147**, 214110 (2017).
[33]K. Nishi, M. L. Kilfoil, C. F. Schmidt, and F. C. MacKintosh, "A symmetrical method to obtain shear moduli from microrheology," Soft Matter **14**, 3716–3723 (2018).
[34]B. Kowalik, J. O. Daldrop, J. Kappler, J. C. F. Schulz, A. Schlaich, and R. R. Netz, "Memory-kernel extraction for different molecular solutes in solvents of varying viscosity in confinement," Phys. Rev. E **100**, 012126 (2019).
[35]M. Fuchs, W. Götze, and M. R. Mayr, "Asymptotic laws for tagged-particle motion in glassy systems," Phys. Rev. E **58**, 3384–3399 (1998).
[36]W. Götze, *Complex Dynamics of Glass-Forming Liquids: A Mode-Coupling Theory*, International Series of Monographs on Physics (Oxford University Press, Oxford, 2009).
[37]S. R. Williams, G. Bryant, I. K. Snook, and W. van Megen, "Velocity autocorrelation functions of hard-sphere fluids: Long-time tails upon undercooling," Phys. Rev. Lett. **96**, 087801 (2006).
[38]H. L. Peng, H. R. Schober, and T. Voigtmann, "Velocity autocorrelation function in supercooled liquids: Long-time tails and anomalous shear-wave propagation," Phys. Rev. E **94**, 060601 (2016).
[39]B. J. Ackerson and L. Fleishman, "Correlations for dilute hard core suspensions," J. Chem. Phys. **76**, 2675–2679 (1982).
[40]M. Fuchs and K. Kroy, "Statistical mechanics derivation of hydrodynamic boundary conditions: the diffusion equation," J. Phys.: Condens. Matter **14**, 9223 (2002).
[41]S. Mandal, L. Schrack, H. Löwen, M. Sperl, and T. Franosch, "Persistent anti-correlations in Brownian dynamics simulations of dense colloidal suspensions revealed by noise suppression," Phys. Rev. Lett. **123**, 168001 (2019).
[42]H. van Beijeren, "Transport properties of stochastic Lorentz models," Rev. Mod. Phys. **54**, 195–234 (1982).
[43]F. Höfling and T. Franosch, "Crossover in the slow decay of dynamic correlations in the Lorentz model," Phys. Rev. Lett. **98**, 140601 (2007).
[44]B. J. Alder and T. E. Wainwright, "Velocity autocorrelations for hard spheres," Phys. Rev. Lett. **18**, 988–990 (1967).
[45]M. H. Ernst, E. H. Hauge, and J. M. J. van Leeuwen, "Asymptotic time behavior of correlation functions," Phys. Rev. Lett. **25**, 1254–1256 (1970).
[46]A. Arbe, P. Malo de Molina, F. Alvarez, B. Frick, and J. Colmenero, "Dielectric susceptibility of liquid water: Microscopic insights from coherent and incoherent neutron scattering," Phys. Rev. Lett. **117**, 185501 (2016).
[47]J. Frenkel, *Kinetic Theory of Liquids*, edited by R. H. Fowler, P. Kapitza, and N. F. Mott (Oxford Univ. Press, London, 1946) pp. 188–249.
[48]G. Tarjus and D. Kivelson, "Breakdown of the Stokes-–Einstein relation in supercooled liquids," J. Chem. Phys. **103**, 3071–3073 (1995).
[49]S. K. Kumar, G. Szamel, and J. F. Douglas, "Nature of the breakdown in the Stokes–Einstein relationship in a hard sphere fluid," J. Chem. Phys. **124**, 214501 (2006).
[50]S. Gupta, J. Stellbrink, E. Zaccarelli, C. N. Likos, M. Camargo, P. Holmqvist, J. Allgaier, L. Willner, and D. Richter, "Validity of the Stokes–Einstein relation in soft colloids up to the glass transition," Phys. Rev. Lett. **115**, 128302 (2015).
[51]A. Dehaoui, B. Issenmann, and F. Caupin, "Viscosity of deeply supercooled water and its coupling to molecular diffusion," Proc. Natl. Acad. Sci. U. S. A. **112**, 12020–12025 (2015).
[52]A. D. S. Parmar, S. Sengupta, and S. Sastry, "Length-scale dependence of the Stokes–Einstein and Adam–Gibbs relations in model glass formers," Phys. Rev. Lett. **119**, 056001 (2017).
[53]J. Mo, A. Simha, and M. G. Raizen, "Brownian motion as a new probe of wettability," J. Chem. Phys. **146**, 134707 (2017).
[54]K. Huang and I. Szlufarska, "Effect of interfaces on the nearby Brownian motion," Nat. Commun. **6**, 8558 (2015).
[55]L. Bocquet and J.-L. Barrat, "Flow boundary conditions from nano- to micro-scales," Soft Matter **3**, 685 (2007).
[56]E. Herrera-Delgado, R. Perez-Carrasco, J. Briscoe, and P. Sollich, "Memory functions reveal structural properties of gene regulatory networks," PLoS Comput. Biol. **14**, e1006003 (2018).
[57]V. Hakim and P. Silberzan, "Collective cell migration: a physics perspective," Rep. Prog. Phys. **80**, 076601 (2017).
[58]K. Kanazawa, T. Sueshige, H. Takayasu, and M. Takayasu, "Derivation of the Boltzmann equation for financial Brownian motion: Direct observation of the collective motion of high-frequency traders," Phys. Rev. Lett. **120**, 138301 (2018).
[59]C. L. E. Franzke, T. J. O'Kane, J. Berner, P. D. Williams, and V. Lucarini, "Stochastic climate theory and modeling," WIREs Clim Change **6**, 63–78 (2014)

METHODS

Generalised Langevin equation. A labelled fluid particle of mass m, position $\boldsymbol{r}(t)$, and momentum $\boldsymbol{p}(t) = m\dot{\boldsymbol{r}}(t)$ obeys the generalised Langevin equation (GLE)[60]:

$$\dot{\boldsymbol{p}}(t) = -\int_0^t \mathrm{d}s\, \gamma(t-s)\, \boldsymbol{p}(s) + \boldsymbol{\xi}(t), \tag{1}$$

where the Brownian force $\boldsymbol{\xi}(t)$ is a stochastic process with zero mean and covariance

$$\langle \boldsymbol{\xi}(t) \otimes \boldsymbol{\xi}(t') \rangle = m k_\mathrm{B} T \gamma(|t-t'|)\, \mathbf{1} \tag{2}$$

to satisfy the fluctuation–dissipation theorem. Rewriting eq. (1) for the the velocity auto-correlation function (VACF), $Z(t) = \langle \boldsymbol{p}(t) \cdot \boldsymbol{p}(0) \rangle / (m^2 d)$, describing momentum relaxation, yields

$$\dot{Z}(t) = -\int_0^t \mathrm{d}s\, \gamma(t-s) Z(s)\,, \quad Z(0) = \frac{k_\mathrm{B}T}{m}\,. \tag{3}$$

Its Fourier–Laplace transform [eq. (8)] provides the link to and the definition of the (complex-valued) memory kernel $\hat{\gamma}(\omega)$,

$$\hat{Z}(\omega) = \frac{k_\mathrm{B}T/m}{-\mathrm{i}\omega + \hat{\gamma}(\omega)}. \tag{4}$$

Linear response. For a mass m driven by a periodic force $\boldsymbol{F}(t) = \boldsymbol{F}_\omega \cos(\omega t)$ with frequency ω and amplitude $\boldsymbol{F}_\omega$, the stationary response $\bar{\boldsymbol{v}}(t)$, averaged over many realisations of the experiment, obeys[60]

$$m\frac{\mathrm{d}}{\mathrm{d}t}\bar{\boldsymbol{v}}(t) = \boldsymbol{F}(t) - \int_{-\infty}^t m\gamma(t-s)\, \bar{\boldsymbol{v}}(s)\, \mathrm{d}s\,, \tag{5}$$

corresponding to eq. (1) after shifting the lower integral boundary to $-\infty$ to ensure relaxation of transients. The upper boundary can be shifted to $+\infty$ with the convention that the response function $\gamma(t<0) = 0$. By linearity of the equation, the solution is of the form $\bar{\boldsymbol{v}}(t) = \mathrm{Re}\big[\boldsymbol{v}_\omega \mathrm{e}^{-\mathrm{i}\omega t}\big]$ with complex amplitude $\boldsymbol{v}_\omega$, and inserting into eq. (5) yields $\boldsymbol{v}_\omega = \hat{\mathcal{Y}}(\omega)\, \boldsymbol{F}_\omega$ in terms of the generalised mobility,

$$\hat{\mathcal{Y}}(\omega) := [-\mathrm{i}\omega m + m\hat{\gamma}(\omega)]^{-1}\,, \tag{6}$$

also referred to as complex-valued admittance. Its central ingredient is the one-sided Fourier transform of the response function, $\hat{\gamma}(\omega) := \int_0^\infty \mathrm{e}^{\mathrm{i}\omega t}\gamma(t)\,\mathrm{d}t$. Comparing to eq. (4), which describes equilibrium correlations, yields the fluctuation–dissipation relation: $\hat{Z}(\omega) = k_\mathrm{B}T\,\hat{\mathcal{Y}}(\omega)$.

Friction describes the resistance to a prescribed velocity, as in Stokes's pendulum experiments[18]. Thus, inverting the above argument, the force response to an oscillatory velocity $\boldsymbol{v}(t) = \boldsymbol{v}_\omega \cos(\omega t)$ has complex amplitude $\boldsymbol{F}_\omega = \hat{\mathcal{Y}}(\omega)^{-1}\, \boldsymbol{v}_\omega$, and we identify $\hat{\mathcal{Y}}(\omega)^{-1}$ as a generalised friction. However, merely the real part describes dissipation and deserves to be called a friction, which is seen from the mean dissipated power: $T_p^{-1}\int_0^{T_p} \boldsymbol{v}(t)\cdot\boldsymbol{F}(t)\,\mathrm{d}t = \mathrm{Re}\big[\hat{\mathcal{Y}}(\omega)^{-1}\big]\,|\boldsymbol{v}_\omega|^2/2$, averaged over a full cycle of length $T_p = 2\pi/\omega$. Thus, we set the dynamic friction as

$$\zeta(\omega) := \mathrm{Re}\big[\hat{\mathcal{Y}}(\omega)^{-1}\big] = m\,\mathrm{Re}\,\hat{\gamma}(\omega)\,; \tag{7}$$

in particular, $\zeta(\omega) \geqslant 0$. This is in line with the conventional (Markovian) Langevin equation, $\dot{\boldsymbol{p}}(t) = -(\zeta_0/m)\,\boldsymbol{p}(t) + \boldsymbol{\xi}(t)$. There, the response is governed by $\hat{\mathcal{Y}}(\omega) = [-\mathrm{i}\omega m + \zeta_0]^{-1}$, implying a static friction, $\zeta(\omega) = \zeta_0$.

Equations (6) and (7) (and variants thereof) are the basis of (passive) microrheology experiments[19–22], which use observations of Brownian motion to infer the friction $\zeta(\omega)$ and $\mathrm{Im}\,\hat{\gamma}(\omega)$ of a probe particle in a complex medium and relate it via the GSER to the local visco-elastic properties. The macroscopic shear viscosity, $\eta_0 = (k_\mathrm{B}T)^{-1}\int_0^\infty C_\Pi(t)\,\mathrm{d}t$, is the Green–Kubo integral of the autocorrelation, $C_\Pi(t) = \langle \delta\Pi^\perp(t)\,\delta\Pi^\perp(0)\rangle/V$, of shear stress fluctuations $\delta\Pi^\perp(t)$, given as an off-diagonal element of the stress tensor[17]; V denotes the sample volume. Similarly by a fluctuation–dissipation relation, the frequency-dependent response coefficient $\hat{\eta}(\omega)$ to oscillatory shear is the Fourier–Laplace transform [eq. (8)] of $C_\Pi(t)/k_\mathrm{B}T$, and thus $\hat{\eta}(\omega\to 0) = \eta_0$.

Mathematical framework. For the harmonic analysis of the autocorrelation function $C(t)$ of a stationary time series, we use the Fourier–Laplace transform

$$\hat{C}(z) = \int_0^\infty \mathrm{e}^{\mathrm{i}zt} C(t)\,\mathrm{d}t\,, \tag{8}$$

which is well-defined for all frequencies z in the upper complex plane, $\mathbb{C}_+ = \{z|\,\mathrm{Im}\,z > 0\}$. Along the imaginary axis, $z = \mathrm{i}y$, it recovers the conventional Laplace transform. For real frequencies ω, the real and imaginary parts of $\hat{C}(\omega)$ describe physically accessible spectra, which are related to each other by Kramers–Kronig integrals[60]; for example, $\mathrm{Re}\,\hat{C}(\omega)$ for fixed ω is determined by the full function $\mathrm{Im}\,\hat{C}(\omega)$. The real part is positive, $\mathrm{Re}\,\hat{C}(\omega) \geqslant 0$, and most importantly, we have the unique Fourier backtransform:

$$C(t) = \frac{1}{\pi}\int_{-\infty}^\infty \mathrm{e}^{-\mathrm{i}\omega t}\,\mathrm{Re}\,\hat{C}(\omega)\,\mathrm{d}\omega\,. \tag{9}$$

If $C(t)$ is n-times continuously differentiable at $t = 0$, this implies sum rules for the spectrum ($k = 0, 1, \ldots, n$):

$$\frac{1}{\pi}\int_{-\infty}^\infty (-\mathrm{i}\omega)^k\,\mathrm{Re}[\hat{C}(\omega)]\,\mathrm{d}\omega = C^{(k)}(0) < \infty\,. \tag{10}$$

In equilibrium, only positive frequencies are needed as $\mathrm{Re}\,\hat{C}(\omega) = \mathrm{Re}\,\hat{C}(-\omega)$, and the integrals are real-valued.

Next, we introduce a memory function of $C(t)$ solely by invoking results from complex analysis[61,62]. $\hat{C}(z)$ as

above is a holomorphic function with $\mathrm{Re}\,\hat{C}(z) \geqslant 0$, i.e., $\mathrm{i}\hat{C}(z)$ is of Herglotz–Nevanlinna type, and $(\mathrm{Im}\,z)\,|\hat{C}(z)|$ bounded in $\mathbb{C}_+$. Suppose that $C(t)$ has a regular short-time expansion, $C(t\to 0) \simeq C_0\big[1-\nu t-\frac{1}{2}at^2\big]$, which implies

$$\hat{C}(z) \simeq C_0(-\mathrm{i}z)^{-1} - \nu C_0(-\mathrm{i}z)^{-2} - aC_0(-\mathrm{i}z)^{-3} \quad (11)$$

for large frequencies, $|z|\to\infty$ with $|\arg z| > \delta$ for some $\delta > 0$. Under these mild requirements, one shows[62]: For given $\hat{C}(z)$ there is a unique memory kernel $\hat{M}(z)$ such that

$$\hat{C}(z) = \frac{C_0}{-\mathrm{i}z + \hat{M}(z)} \quad (12)$$

with $\mathrm{i}\hat{M}(z)$ of Herglotz–Nevanlinna type and $\hat{M}(z) \simeq \nu + a/(-\mathrm{i}z)$ as $|z|\to\infty$. In particular, $\hat{M}(z)$ corresponds to the autocorrelation function of another (*a priori* unknown) observable. Iterating the argument yields the continued-fraction representation of $\hat{C}(z)$, well-known from the Zwanzig–Mori projection formalism[17].

In the context of the VACF, one puts $C_0 = v_{\mathrm{th}}^2$, $\nu = 0$, and $a = \omega_0^2$ and infers for the memory kernel $\hat{M}(z) =: \hat{\gamma}(z)$ that $\mathrm{Re}\,\hat{\gamma}(z) \geqslant 0$ and $\hat{\gamma}(z) \simeq \omega_0^2/(-\mathrm{i}z)$ as $|z|\to\infty$. This justifies eq. (4) independently of the notion of a GLE, after taking z along the real line.

By means of eq. (9), $\hat{\gamma}(z)$ specifies the memory function $\gamma(t)$, which has a physical interpretation as the autocorrelator of the fluctuating acceleration $\boldsymbol{\xi}(t)/m$ in eq. (1), divided by v_{th}^2. At low frequencies, $m\hat{\gamma}(z\to 0) = \zeta_0$ implies a Green–Kubo relation for the hydrodynamic friction:

$$\zeta_0 = m\int_0^\infty \gamma(t)\,\mathrm{d}t\,. \quad (13)$$

Short-time expansion. The smoothness of physical molecular trajectories, being solutions to Newton's equations, allows for a rigorous short-time expansion of the VACF. Combining with the time-reversal symmetry in equilibrium, $Z(t) = Z(-t)$, only even powers in t contribute and one obtains $Z(t\to 0) \simeq k_{\mathrm{B}}T\sum_{k=0}^\infty c_k t^{2k}/(2k)!$ with Taylor coefficients c_k given from equilibrium matrix elements of powers of the underlying Liouville operator[63]. To connect with the notation of the main text, $c_0 = 1/m$, $c_1/c_0 = -\omega_0^2$, and we put $c_2/c_0 =: \Omega^4$. Fourier–Laplace transforming term by term yields the high-frequency expansion of $\hat{Z}(\omega)$ and thus of $\hat{\mathcal{Y}}(\omega) = (k_{\mathrm{B}}T)^{-1}\hat{Z}(\omega)$, which is purely imaginary: $\hat{\mathcal{Y}}(\omega\to\infty) \simeq \sum_{k=0}^\infty c_k\,(-\mathrm{i}\omega)^{-1-2k} = c_0/(-\mathrm{i}\omega) + c_1/(-\mathrm{i}\omega)^3 + \ldots$. Using eq. (7), we have $\zeta(\omega) = |\hat{\mathcal{Y}}(\omega)|^{-2}\,\mathrm{Re}\,\hat{\mathcal{Y}}(\omega)$, which implies that for high frequencies the friction vanishes, $\zeta(\omega)\equiv 0$, at all orders in $\omega\to\infty$. A similar situation is familiar from calculus text books: $f(x) = \mathrm{e}^{-1/x}$ has a Taylor series $f(x)\equiv 0$ at $x = 0$; the radius of convergence is 0.

The expansion of $\hat{\mathcal{Y}}(\omega)$ can be represented as a continued fraction that has the same large-ω asymptotics up to terms of order ω^{-5}:

$$\hat{\mathcal{Y}}(\omega) \simeq 1/\big\{-\mathrm{i}\omega m + m\omega_0^2/\big[-\mathrm{i}\omega + \omega_1^2/(-\mathrm{i}\omega + \ldots)\big]\big\}\,, \quad (14)$$

introducing $\omega_1^2 := \big(\Omega^4 - \omega_0^4\big)/\omega_0^2$ for brevity. This truncation is an excellent description of our data for $\hat{\mathcal{Y}}''(\omega)$ at high frequencies, with ω_0 and Ω obtained from fits to $Z(t)$, see fig. 3d–f. For the memory kernel $\hat{\gamma}(\omega)$, one reads off

$$\hat{\gamma}(\omega\to\infty) = \omega_0^2/(-\mathrm{i}\omega) - \omega_0^2\omega_1^2/(-\mathrm{i}\omega)^3 + \mathcal{O}\big(\omega^{-5}\big)\,, \quad (15)$$

using eq. (6), implying for the memory function in time domain:

$$\gamma(t\to 0) = \omega_0^2\,\big[1 - \omega_1^2 t^2/2\big] + O\big(t^4\big). \quad (16)$$

Long-time tails. In an unbounded fluid, momentum conservation leads to persistent velocity correlations, $Z(t\to\infty) \simeq v_{\mathrm{th}}^2(t/\tau_\infty)^{-3/2}$, which was explained in terms of hydrodynamic backflow and diffusion of a momentum vortex[17,44,45]. The tail induces a small-ω singularity in the frequency domain[64], which reads for the memory kernel: $m\hat{\gamma}(\omega\to 0) \simeq \zeta_0\big[1 + (\tau_\infty\zeta_0/m)\sqrt{-4\pi\mathrm{i}\omega\tau_\infty}\big)\big]$, using eq. (4) and the hydrodynamic friction $\zeta_0 := m\hat{\gamma}(0) = k_{\mathrm{B}}T/\int_0^\infty Z(s)\,\mathrm{d}s$.

In the framework of the creeping flow equations, Stokes found[18]

$$m\hat{\gamma}(\omega\to 0) \simeq 6\pi\eta_0 a(1 + \sqrt{-\mathrm{i}\omega\tau_{\mathrm{fl}}}) - \mathrm{i}\omega m_{\mathrm{fl}}/2 \quad (17)$$

in terms of the vorticity diffusion time τ_{fl} and an effective particle mass m_{fl}; matching with the previous expression for the asymptote of $\hat{\gamma}(\omega)$, one identifies $\tau_{\mathrm{fl}} = 4\pi(\zeta_0/m)^2\tau_\infty^3$. The real part yields the dynamic friction,

$$\zeta(\omega\to 0) \simeq 6\pi\eta_0 a(1 + \sqrt{\omega\tau_{\mathrm{fl}}/2})\,, \quad (18)$$

showing that its macroscopic limit, $\zeta_0 = 6\pi\eta_0 a$, is approached from above as $\omega\to 0$ (see fig. 3b). For water and the supercooled liquid, a different type of power law decay, $Z(t) \sim -t^{-5/2}$, was found (fig. 3e,f).

For a general long-time tail of the VACF, $Z(t) \sim t^{-\sigma}$ with $\sigma > 1$, the memory function $\gamma(t)$ asymptotically inherits a power-law decay with the same exponent, but of opposite sign[65]:

$$\gamma(t) \simeq -\hat{\gamma}(0)^2 Z(t)/Z(0)\,, \quad t\to\infty\,; \quad (19)$$

which follows from eq. (3) and by invoking a Tauber theorem[64]. Without any adjustable parameter, the prediction is in excellent agreement with our data for $\gamma(t)$ in case of the LJ fluid. Inspection of a few examples (figs. 4d,e and 5c) suggests that, in order to accommodate the sign change of the tail, the number of zero crossings (knots) in $\gamma(t)$ is increased by one relative to $Z(t)$.

Analytically solvable example. Consider the following analytically tractable model for the VACF:

$$Z(t) = \frac{v_{\mathrm{th}}^2}{1+(t/\tau)^2}\,, \quad v_{\mathrm{th}}^2 = k_{\mathrm{B}}T/m\,, \tag{20}$$

with relaxation time τ and thermal velocity v_{th} (fig. S1d). It favourably combines the physically required smoothness at $t = 0$ and time-reversibility, $Z(t) = Z(-t)$, with a power-law decay at long times, $Z(t \to \infty) \simeq v_{\mathrm{th}}^2 (t/\tau)^{-2}$; in particular, only even powers of t contribute to the the short-time expansion: $Z(t \to 0) \simeq v_{\mathrm{th}}^2 \left[1 - (t/\tau)^2 + O(t^4)\right]$. From the one-sided Fourier transform of $Z(t)$, we obtain the real and imaginary parts of $\hat{Z}(\omega)$ as $\mathrm{Re}\,\hat{Z}(\omega) = D_\infty \mathrm{e}^{-|\omega\tau|}$ and $\mathrm{Im}\,\hat{Z}(\omega) = D_\infty[\mathrm{e}^{-\omega\tau}\,\mathrm{Ei}(\omega\tau) - \mathrm{e}^{\omega\tau}\,\mathrm{Ei}(-\omega\tau)]/\pi$, being even and odd functions in ω, respectively (fig. 5a). Here, $\mathrm{Ei}(\cdot)$ denotes the exponential integral, and $D_\infty = v_{\mathrm{th}}^2 \tau\pi/2$ is the long-time limit of the diffusivity, $D(t) = \int_0^t Z(s)\,\mathrm{d}s = v_{\mathrm{th}}^2 \tau \arctan(t/\tau)$. Given $Z(\omega)$, the explicit expression for the complex memory kernel $\hat{\gamma}(\omega)$ and the friction $\zeta(\omega)$ follow from eqs. (4) and (7), see fig. 5b. The low- and high-frequency asymptotes correspond to $\zeta(\omega \to 0) \simeq \zeta_0(1 + |\omega\tau|)$ and $\zeta(\omega \to \infty) \simeq \zeta_0 (\pi\omega\tau/2)^2\, \mathrm{e}^{-|\omega\tau|}$, respectively, with $\zeta_0 = k_{\mathrm{B}}T/D_\infty$. The friction attains its maximum $\approx 1.2\zeta_0$ near $\omega_{\max} \approx 0.892\tau^{-1}$ and falls off rapidly for larger ω; the position of the maximum of $\mathrm{Im}\,\hat{\gamma}(\omega)$ sets the onset frequency $\omega_c \approx 4.01\tau^{-1}$. The memory function $\gamma(t)$ is obtained numerically from $\zeta(\omega)$ using eq. (9), with the short- and long-time asymptotes $\gamma(t \to 0) \simeq 2\tau^{-2}[1 - 5(t/\tau)^2]$ and $\gamma(t \to \infty) \simeq -(\zeta_0/m)^2 (t/\tau)^{-2}$, respectively (fig. 5c).

Adapted Filon algorithm. The computation of the frequency-dependent friction requires a robust numerical Fourier transform, for which we developed a physics-enriched version of Filon's quadrature formula. The goal is to evaluate $\hat{f}(\omega) = \int_0^\infty \mathrm{e}^{\mathrm{i}\omega t} f(t)\,\mathrm{d}t$ for a function $f(t)$ sparsely sampled on an irregular grid $t_0 = 0, t_1, \ldots, t_n$ for an arbitrary set of frequencies (ω_j). The idea of Filon's algorithm is to interpolate $f(t)$ by elementary functions between the grid points (usually parabolas), thereby reducing the Fourier integral to a finite sum of integrals, for which analytic expressions exist. Anticipating that the normal physical decay of correlation functions is exponential, we approximate $f(t) \approx a_k \mathrm{e}^{-\gamma_k t}$ in the interval $[t_k, t_{k+1}]$ with a_k and γ_k fixed by $f(t_k)$ and $f(t_{k+1})$. Then,

$$\hat{f}(\omega) \approx \int_0^{t_1} \mathrm{e}^{\mathrm{i}\omega t} f(t)\,\mathrm{d}t + \sum_{k=1}^{n-1} \int_{t_k}^{t_{k+1}} a_k \mathrm{e}^{(\mathrm{i}\omega - \gamma_k)t}\,\mathrm{d}t + \int_{t_n}^{\infty} a_n \mathrm{e}^{(\mathrm{i}\omega - \gamma_n)t}\,\mathrm{d}t\,. \tag{21}$$

Spurious low-frequency oscillations of the transform are removed by smoothly truncating the integral at t_n, here by assuming a terminal exponential decay of $f(t)$, which leads to the last term on the r.h.s. of eq. (21). In order to preserve the short-time properties of $f(t)$ we fit a polynomial in t^2 to the first few data points and solve the integral analytically; this improves the high-frequency behaviour of $\hat{f}(\omega)$.

The dynamic friction $\zeta(\omega)$ and the memory function $\gamma(t)$ are obtained from MSD data as follows (fig. 2): The timescale-dependent diffusion coefficient, $D(t) := \partial_t \mathrm{MSD}(t)/6$, is obtained from numerical differentiation. In all cases studied, it grows out from zero, has a maximum, and converges slowly towards the long-time diffusion constant $D_\infty = D(t \to \infty)$, see supplemental fig. S1. Using the above algorithm, we compute[66] $\hat{Z}(\omega) = D_\infty - \mathrm{i}\omega \int_0^\infty \mathrm{d}t\, \mathrm{e}^{\mathrm{i}\omega t}[D(t) - D_\infty]$. Then, $\zeta(\omega)$ is given by eq. (4) and is transformed back to the time domain with the same algorithm [eq. (9)]; in particular, we use again a smooth, exponential cutoff. In fig. 5, the numerical procedure is successfully tested against the analytical model with high accuracy.

Deconvolution in time domain. Inversion of the convolution in eq. (3) yields the memory function $\gamma(t)$ directly[67], without resorting to the frequency domain. Numerically, it is not easy to obtain accurate and robust results, and a variety of algorithms have been developed, see Ref.[34] for a comparative study. The presence of $\dot{Z}(t)$ in eq. (3) is removed by integration, yielding $Z(t) = Z(0) - \int_0^t \mathrm{d}s\, G(t-s) Z(s)$ with the integrated memory $G(t) := \int_0^t \mathrm{d}s\, \gamma(s)$. Discretising on a uniform time grid, $t_i = i\Delta t$ $(i = 0, 1, \ldots)$, and employing the trapezoidal rule for the integral, a recursion relation for $G_i := G(t_i)$ with the initial value $G_0 = 0$ follows[34]:

$$G_i = \frac{1 - Z_i/Z_0}{\Delta t/2} - 2\sum_{j=1}^{i-1} G_j Z_{i-j}/Z_0\,, \quad i \geqslant 1\,. \tag{22}$$

Going beyond Ref.[34], we introduce a predictor–corrector scheme to stabilise the numerical solutions: In the predictor step, one evaluates G_i^* and G_{i+1}^* from eq. (22). Afterwards, the weighted average $G_i := (G_{i-1} + 3G_i^* + G_{i+1}^*)/5$ manifests itself as the corrector step. Results for $G(t)$ can be found in fig. S2. Finally, the memory function $\gamma(t) = \partial_t G(t)$ is obtained by central differences. If one starts from MSD data on a sparse (e.g., geometrically spaced) time grid, a cubic spline interpolation of the MSD in the variable t^2 is suitable to sample $Z(t)$ on a uniform grid of up to 10^5 points.

Molecular dynamics simulations. Simulations of liquid water were performed with the GROMACS 5.1 package[68] using the SPC/E water model. The system of 3,007 molecules was equilibrated at 300 K and 1 bar following standard procedures[34]. Correlation functions were obtained from NVE simulations over 275 ps with the velocity-Verlet integrator and a time step of 1 fs, using double floating-point precision to achieve good energy conservation.

For the other two liquids, we used the massively parallel software *HAL's MD package* (version 1.0-α6)[69], permitting the sampling of dynamic correlations on a sparse time grid and featuring smoothly truncated potentials to virtually eliminate any energy drift. The mono-atomic fluid consists of 10^5 particles interacting pairwise via the LJ potential, $U(r) = 4\varepsilon\big[(r/\sigma)^{-12} - (r/\sigma)^{-6}\big]$, truncated for $r \geqslant 2.5\sigma$; a unit of time is defined by $\tau_{\mathrm{LJ}} := \sqrt{m\sigma^2/\varepsilon}$. Equilibration in the NVE ensemble at number density $\varrho = 0.8\sigma^3$ and thermal energy $k_{\mathrm{B}}T = 1.3\varepsilon$ followed the protocol in ref.[70]. The supercooled liquid was realised by a Kob–Andersen 80:20 binary mixture[71] of 64,000 LJ beads at $\varrho = 1.2\sigma^{-3}$ and $k_{\mathrm{B}}T = 0.6\varepsilon$, equilibrated over a time span of $9{,}000\,\tau_{\mathrm{LJ}}$, and we traced the species of the larger particles. The simulations generate trajectories $\boldsymbol{r}(t)$ of an ensemble of labelled particles for each fluid; our main observable is the mean-square displacement $\mathrm{MSD}(t) := \big\langle|\boldsymbol{r}(t) - \boldsymbol{r}(0)|^2\big\rangle$ for lag time t. For both liquids, single-particle MSDs were averaged from 10 production runs, each over 10^8 integration steps of length $0.001\,\tau_{\mathrm{LJ}}$.

Control simulations of a single particle in its pinned cage are based on an equilibrated sample of the LJ fluid with 10^6 particles. MSDs were recorded after equilibration of the mobile particle in its static environment over $100\,\tau_{\mathrm{LJ}}$ and were averaged over 10^6 different cages, computed in parallel, to remove spurious oscillations. Technically, the setup was realised by making two initially identical copies of the fluid interact with each other: the first copy contains the immobile matrix, the second one the tracers (not interacting with each other).

Acknowledgements. This research has been funded by Deutsche Forschungsgemeinschaft (DFG, German Research Foundation) through the grant SFB 1114 (projects B03 and C01) and under Germany's Excellence Strategy – MATH+ : The Berlin Mathematics Research Center (EXC-2046/1) – project ID: 390685689 (subproject EF4-4). Further funding by the European Research Council (ERC Advanced H 2020 Grant "NoMaMemo") is gratefully acknowledged.

Author contributions. AS, RN, and FH conceived the project and wrote the manuscript. BK and FH performed the simulations, and AS and FH analysed the data. AS carried out the analytical work. All authors discussed the results and implications and commented on the manuscript at all stages.

REFERENCES

[60] R. Kubo, M. Toda, and N. Hashitsume, *Statistical Physics II: Nonequilibrium Statistical Mechanics* (Springer, Berlin, Heidelberg, 1991).
[61] G. Teschl, *Mathematical methods in quantum mechanics: with applications to Schrödinger operators*, 2nd ed. (Am. Math. Soc., Providence, RI, 2014).
[62] T. Franosch, J. Phys. A: Math. Theor. **47**, 325004 (2014).
[63] J. P. Boon and S. Yip, *Molecular Hydrodynamics* (Dover Publications, Inc., New York, 1991) reprint.
[64] J. Karamata, J. reine angew. Math. **164**, 27 (1931).
[65] N. Corngold, Phys. Rev. A **6**, 1570 (1972).
[66] T. Franosch, M. Spanner, T. Bauer, G. E. Schröder-Turk, and F. Höfling, J. Non-Cryst. Solids **357**, 472 (2011).
[67] B. J. Berne, M. E. Tuckerman, J. E. Straub, and A. L. R. Bug, J. Chem. Phys. **93**, 5084 (1990).
[68] B. Hess, C. Kutzner, D. Van Der Spoel, and E. Lindahl, J. Chem. Theory Comput. **4**, 435 (2008).
[69] P. H. Colberg and F. Höfling, Comput. Phys. Commun. **182**, 1120 (2011); "Highly Accelerated Large-scale Molecular Dynamics package," (2007–2019), `https://halmd.org`.
[70] S. Roy, S. Dietrich, and F. Höfling, J. Chem. Phys. **145**, 134505 (2016).
[71] W. Kob and H. C. Andersen, Phys. Rev. Lett. **73**, 1376 (1994)

SUPPLEMENTAL MATERIAL

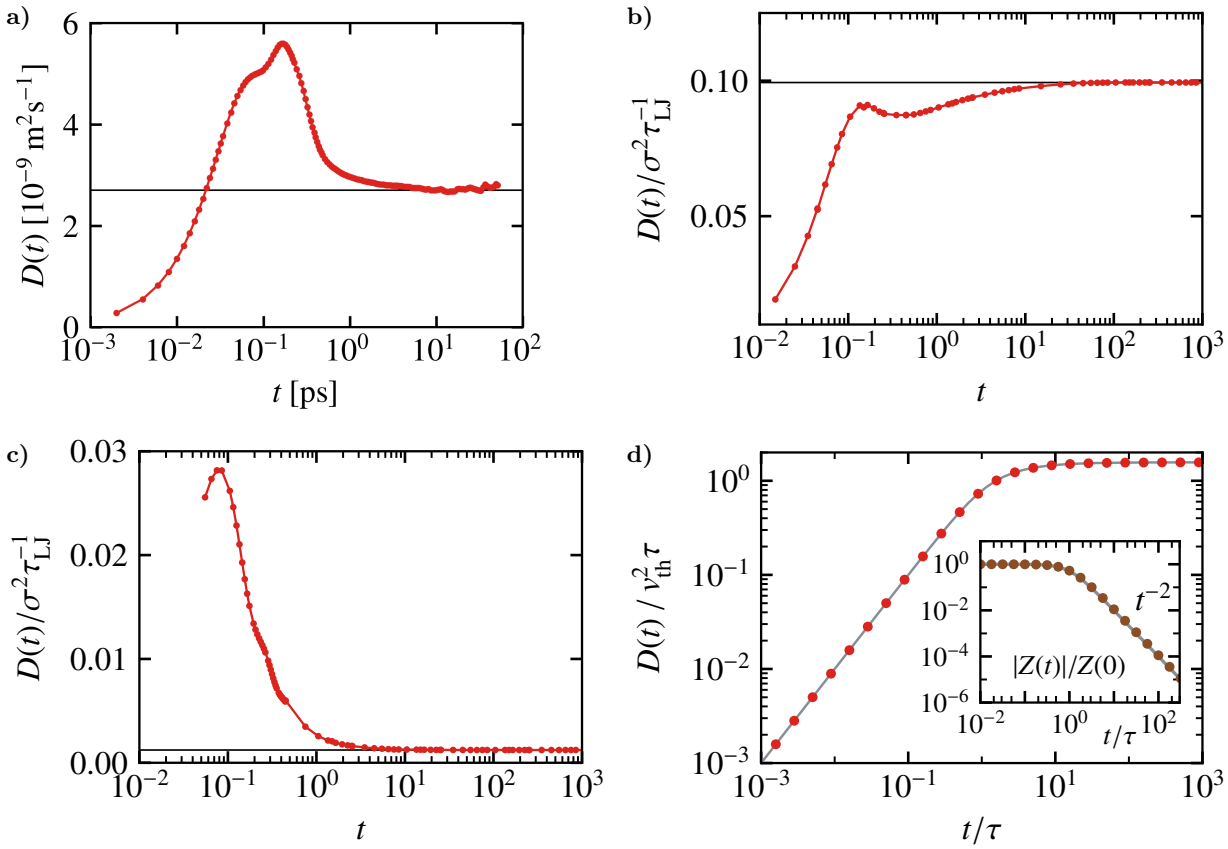

FIG. S1. Timescale-dependent diffusion coefficient $D(t) = \partial_t \mathrm{MSD}(t)/6$ for (panel a) liquid water, (b) a Lennard-Jones fluid, (c) a supercooled Kob–Andersen mixture, and (d) the analytical example. In panel (d), symbols represent data points used for the numerics (only every 5th point is drawn for clarity), solid lines correspond to the analytical expressions.

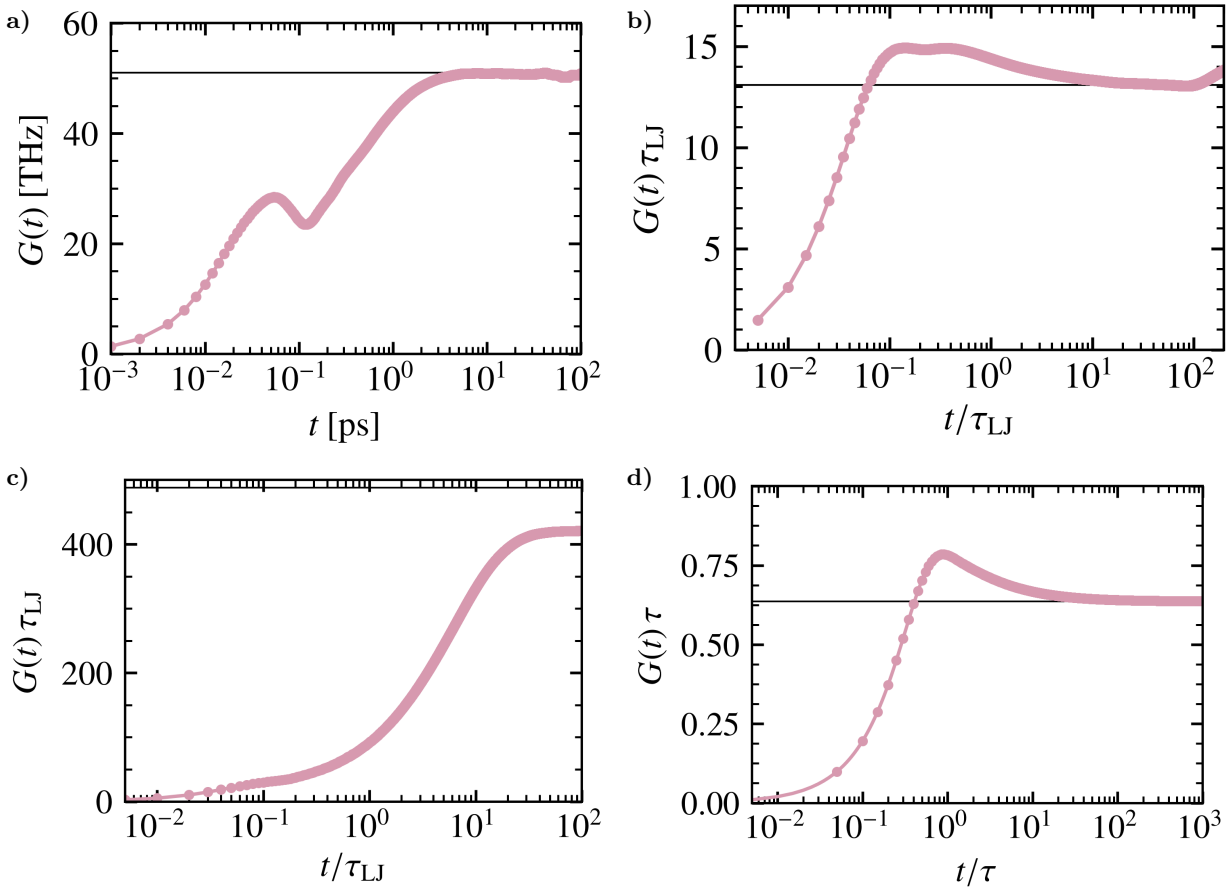

FIG. S2. Integral $G(t) = \int_0^t \gamma(s)\,\mathrm{d}s$ of the memory function for (panel a) liquid water, (b) a Lennard-Jones fluid, (c) a supercooled Kob–Andersen mixture, and (d) the analytical example. The long-time limit $G(t \to \infty) = \zeta_0/m$ is indicated by the horizontal line.